sustainability

MDPI

Article

Thermal Evaluation of a Double-Pass Unglazed Solar Air Heater with Perforated Plate and Wire Mesh Layers

Afaq Jasim Mahmood

Department of Power Mechanics Techniques, Institute of Technology Baghdad, Middle Technical University, Baghdad 10001, Iraq; Dr.Afaq_jasem100@mtu.edu.iq

Received: 2 March 2020; Accepted: 20 April 2020; Published: 30 April 2020

Abstract: In this study, an experimental outdoor investigation of the thermal efficiency and outlet air temperature was conducted on an unglazed, double-pass, solar air heater with a perforated absorber plate and packing wire mesh layers as a supplemental absorbent area. This was done to observe their effects on the thermal performance of the solar air heater. The double-pass collector was constructed with a bed height of 0.05 m, and a collection area of 1.5 m^2. The height of the upper channel was fixed at 0.015 m to improve the thermal efficiency, and the outlet temperature at air flow rates between 0.003 and 0.018 kg/s. The collector was mounted with a slope of 42° facing south, to maximize the intensity of solar irradiance during winter. The effects of the air flow rate, ambient temperature, inlet temperature, outlet temperature, and solar intensity were experimentally investigated. The results showed that thermal efficiency could be improved by increasing the air flow rate, where the highest thermal efficiency achieved was 86% at 0.018 kg/s. However, the temperature difference was increased to a maximum value of 38.6 °C, when the air flow rate was decreased to 0.003 kg/s. Furthermore, the results demonstrated a significant improvement in the thermal efficiency and outlet temperature; and when compared with previous research, the experimental results and the predictions for the outlet temperature using the theoretical model agreed.

Keywords: solar air heater; double pass; thermal efficiency; perforated absorber plate; wire mesh layers

1. Introduction

Energy is vital to human life. The rapid increase in the global economy and technological development, as well as population growth, has increased the demand for energy. Most energy is produced from nonrenewable sources, such as fossil fuel, because of the low cost of production and large supply. The fossil fuel production generates various hazards to the environment, and to human health—such as acid rain, global warming, and photochemical smog [1].

Utilizing a solar energy system for heating space, such as using solar air collectors, is a clean technique to decrease CO_2 emissions and resource consumption [2]. This type of heating system is low-cost and easy to maintain, but has the disadvantage of low thermal efficiency [3]. Solar air collectors have several advantages compared to application of other, liquid-type solar energy systems, such as no freezing or corrosion problems, less maintenance required, and ability to use a perforated plate system (which provides fresh air that improves the indoor air quality).

Solar air heaters can be classified into two basic modes: glazed collectors and unglazed transpired collectors. The unglazed transpired collector is relatively new solar technology that was developed in the 1980s for ventilation air heating. The absorber part of the unglazed transpired collector is perforated so that ambient air is continuously withdrawn through the perforations [4]. Much technological

and financial effort has gone into research on improving the thermal efficiency of solar collectors, because of their use as a renewable energy resource, lack of implementation, and environmental friendliness [5]. Multiple factors affect the solar collector efficiency, such as meteorological parameters (ambient temperature, wind speed, and solar intensity); design parameters (collector materials, size, and type); flow parameters (flow pattern, air flow rate, mode of flow, collector cover, absorber shape); and material (e.g., black-colored wood, aluminum, thin steel plate) [6]. The most important parameters that affect thermal efficiency are the absorber plate, the collector cover, and the air flow pattern inside the collector [7].

Several investigators have undertaken experiments regarding heat transfer analysis of solar energy systems, such as the unglazed transpired solar heaters without cover glasses that have been studied by Bhushan and Singh [8]. One theoretical investigation analyzed the thermal efficiency of the unglazed transpired solar heaters [9], while another predicted theoretical efficiency as a function of wind speed, suction velocity, ambient temperature, and radiation [10]. It has been found that a hole's pitch and diameter are affected by heat transfer between the perforated absorber plate and passing air through holes [11]. Another study found that the non-uniform air flow caused by using porous media has a greater heat transfer coefficient than that in uniform air flow without porous media; and that for the same collector, it was better to put porous media at the lower part of a double pass solar collector [12]. Empirical relations for heat transfer coefficients were estimated [13]. A numerical model was developed to analyze the efficiencies of unglazed transpired solar collectors. Decker et al. [14] improved the model from Bhushan and Singh [8], and developed a wider range and higher accuracy model to predict the efficiencies of collectors.

A double-pass counter-flow was conducted to improve the thermal performance of the transpired solar heater [15]. Several studies have shown that the double-pass solar collectors were more efficient than single-pass solar heaters [16]. Packed bed lower or upper absorber plates were used for improving thermal efficiency and outlet temperature [17]. The model for the solar collector with a double-pass or counter-flow indicates that increasing the air flow proportionally increases the percentage temperature rise of the channel [18]. Some researchers investigated the thermal performance of a double-pass, counter-flow solar collector with porous material in the second air passage [19]; they studied the behavior of the solar collector with and without porous media, and compared them according to various governing parameters, such as the air mass flow rate, inlet air temperature, spacing between the top cover and absorber plate, and the intensity of the solar radiation [20]. The solar heater achieved a higher thermal efficiency with porous media than without porous media. The thermal conductivity of the porous media was found to have a significant effect on the thermal performance of the solar heater [21]. The thermal efficiencies of double-pass air heaters with matrix absorber lower channels were 25% higher than collectors without a matrix absorber [22].

A double-pass solar heater, with wire mesh layers and quarter perforated cover plate, was presented by Nowzari et al. [23], and the maximum temperature value reached was 46 °C. Unglazed solar transpired collector systems offer potential low cost and high efficiency. While numerous authors reported favorable results [24] after improving the efficiency of the transpired collectors, some experimentally and numerically studied the unglazed transpired collector in cold claimant for heating space [25]. Moreover, some researchers used transpired solar collectors with perforating corrugated plates [26], or protruded absorber plates with roughened solar air heaters [14], and others were invented, such as the absorber plate with circular holes, slit-like perforations, multi v-shaped gap ribs, and roughened protrusions [27], enabling them to save a large amount of thermal energy.

As seen from previous studies, researchers are working to improve the performance of the thermal efficiency and outlet temperature of the solar thermal processes. Thus, the aim for this research was to invent new designs using a double-pass unglazed transpired collector with a perforated plate and wire mesh packed, as shown in Figures 1 and 2. The important contribution of this research was using wire mesh layers (increasing the absorbing area) and a perforated absorber plate, and the double-pass counter-flow collector in the duct, to enhance thermal performance. The purposes of the

used double-pass, counter-flow collector include: First, increasing the air path to gain more heat and minimize heat loss to the surroundings; and second, maximizing heat transfer to the airstream in the upper channel.

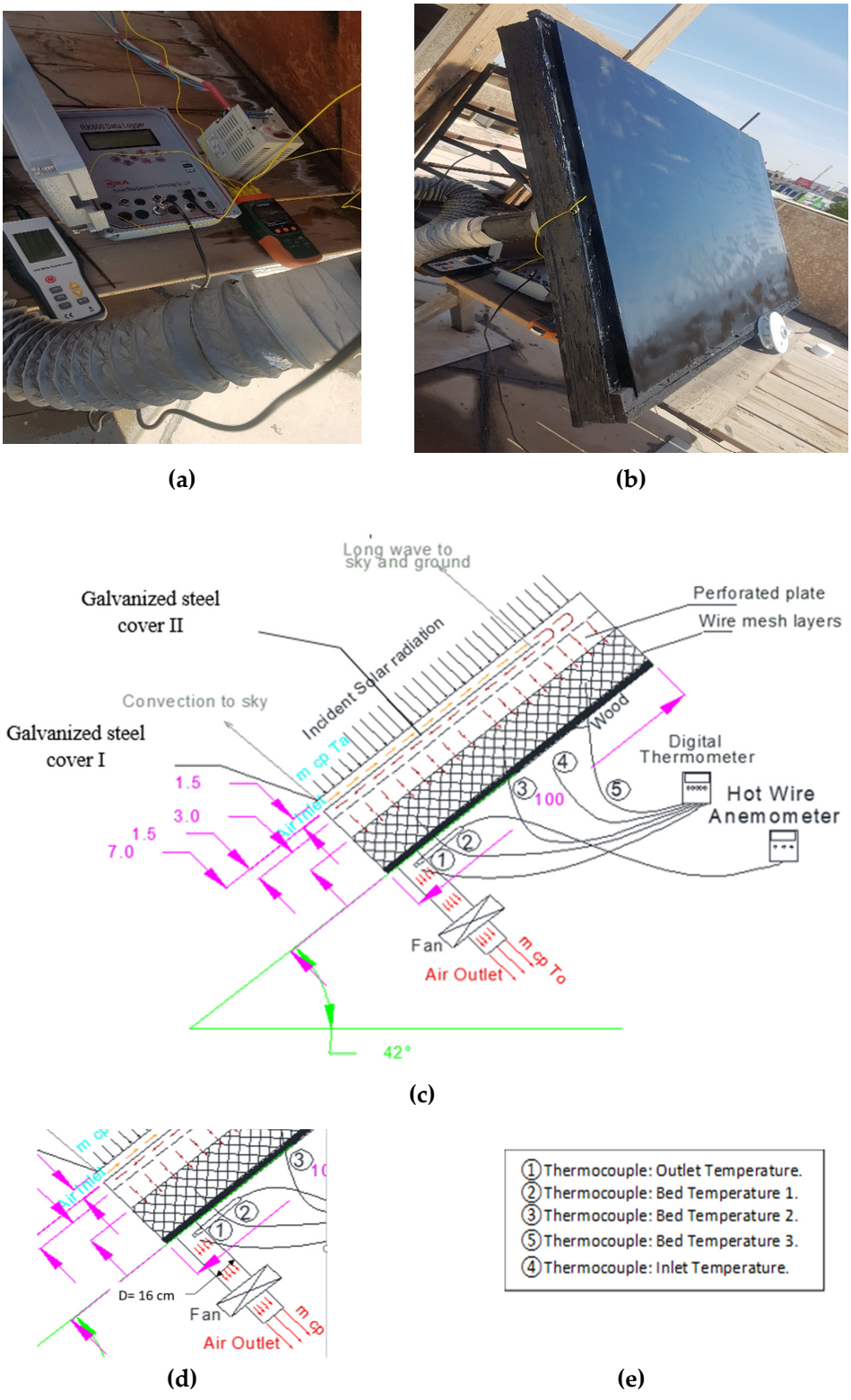

Figure 1. (**a**,**b**) Photos of a solar energy system; (**c**,**d**) scheme of the studied double-pass unglazed solar energy system; (**e**) sensor number.

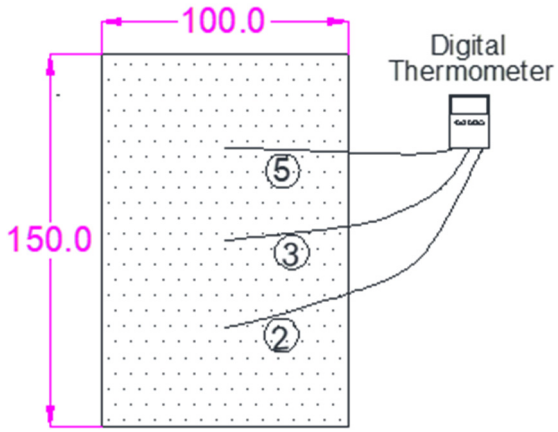

Figure 2. The scheme shows the location of thermostable for measuring bed temperatures.

2. Experimental Setup

2.1. Construction and Design

The structure of the new transpired flat-plate collector was constructed and performed in Baghdad, Iraq 33.3152° N, 44.3661° E, double-pass-counter flow collector is shown in Figure 1. The double pass collector made of wood, with an area of 1.5 m^2 (1.5 m long and 1 m width). All edges and bottom of the collector were thermally insulated, except the upper side of the collector. Two ordinary panes of the plate (steel galvanized), the thickness of 4 mm were fixed parallel and upper the collectors to allow the inlet air to pass through these two plates in a space of 1.5 cm (upper channel), the flow then reversed direction to inter the bottom of the collector, lower channel (lower channel: The distance from Galvanized steel cover II to the back bed), high of 7 cm. The main components of the collectors were the six aluminum wire mesh layers (square hole area 2.2 × 2.2 mm^2) and galvanized steel perforated absorber plate, hole diameter 2 mm and pitch 4 mm. The collectors' bed, perforated plate and wire mesh layers were painted black before installation to increase the absorbing heat from the solar rays and improving the efficiency. A blower of 0.75 kW was connected with collectors by flexible (8 cm diameter) pipe, vary air mass flow rate from 0.003 to 0.018 kg/s controlled by controller speed inverter model: SV008iC5-1, 0.01−400 Hz, 5 A was fixed with air blower electricity, for more detail see Table 1.

Table 1. The characteristics of the equipment used during the tests.

Equipment	Characteristics
Solar heater location	Baghdad, Iraq, (33° N and 44° E)
Solar heater slope and orientation	42° degree, South.
Solar heater dimensions	1.5 m × 1.0 m × 0.07 m
Perforated absorber plate	2 mm diameter, Pitch 4 mm
Wire mesh layers	porosity Φ = 0.88, absorptivity 0.96
Galvanized steel cover no.	2
Centrifugal fan	0.75 kW, Model 135C16A
Hot wire anemometer	HT-9829, 60–90 mA
Temp. data-logger (EXTECH)	accuracy of ± (0.4% + 1 °C), model SDL200
Pyranometer	RK200-03, SN:R18021068, Range: 0–2000 W/m^2.

2.2. Methodology

In this study, outdoor experiments setup was conducted and developed in Baghdad, Iraq. Solar air collector was thermal performance and tested for five cloudless days in April 2019, the slope of 42° facing south, thus, maximizing the solar intensity for winter days. The measurement equipment was a data-logger (EXTECH), an accuracy of ± (0.4% + 1 °C), model SDL200, using for obtained inlet, plenum and outlet temperatures and Pyranometer placed lower to the collector to sense the global

solar irradiance (Pyranometer RK200-03, 0–2000 w/m^2 Range, SN: R18021068) used for measuring solar intensity. The air velocity was measured and taken manually by HT-9829, 60–90 mA, hot wire anemometer, and solar intensity and temperatures were registered automatically every 30 min a day. A vacuum blower power of 0.75 kW, model 135C16A was used to discharge five air flows during five-day work, from 0.003 to 0.018 kg/s. A blower speed controlled by using the inverter drive speed control model: SV008iC5-1, 5 A, 0.01–400 Hz.

3. Instantaneous Efficiency of the Solar Collector

To evaluate the performance of the solar heater system, the first law of thermodynamic was applied, and the thermal efficiency was defined as the ratio of the useful energy to receive energy, and the useful energy was defined as the thermal energy, and receives energy as heat flux or solar radiation energy.

$$Thermal\ Efficiency\ =\ \frac{Useful\ Energy\ Gain}{Received\ Energy} \tag{1}$$

$$\eta_{th}\ =\ \frac{\dot{m}\ c_p(T_o - T_i)}{I\ A_c} \tag{2}$$

where useful energy gain and received energy in (W), ṁ is the air flow rate (kg/sec), C_p is the specific heat of the air (kJ/kg K), A_c is the collector area in (m^2), (T_o) is the outlet air temperature (°C), and T_i is the inlet air temperature (°C) [19,20].

Equation (2) can be simplified to:

$$\eta_{th}\ =\ \frac{\dot{m}c_p}{A_c}.\ \frac{(T_o - T_i)}{I} \tag{3}$$

It is clear from Equation (3), that there is a linear relationship between η_{th} and (T_o−T_i)/I, the positive slope given with $\frac{\dot{m}c_p}{A_c}$.

The performance of flat plate solar collector operating under steady conditions can be successfully described Equation (4). Thermal efficiency is solved heat removal coefficient (F_R) as shown [19]:

$$\eta_{th}\ =\ F_R\left[(\tau\alpha) - (U_L)\frac{(T_i - T_a)}{I}\right] \tag{4}$$

where ($\tau\alpha$) is the effective transmittance absorbance product, (U_L) is the overall heat loss coefficient in W/ (m^2 K), and (F_R) is the collector heat removal factor which relays the actual useful energy gain to the useful gain that the collector surface was at the air inlet temperature. For this state Equation (4) gives a linear relationship between and (T_i−T_a)/I, but a negative slope of [−(F_R U_L)/I], and the origin order at F_R ($\tau\alpha$).

4. Experimental Results

4.1. Ambient Temperature, Relative Humidity and Solar Intensity

Daily values of ambient air temperature, relative humidity and solar radiation incident were registered from 08:00 to 16:00 within a period between 23–27 April 2019 at Baghdad, Iraq. Figure 3, shows the total average for those parameters within the five days of the experimental work. The average ambient air temperature was increased slightly from 11 °C, with a solar intensity value of 340 W/m^2, in the morning to 18 °C, with a solar intensity value of 110 W/m^2, at the end of the day. The average maximum solar intensity was 820 W/m^2 at noon. The average relative humidity dropped, as opposed to the average ambient air temperature, during the day from 08:00 a.m. to 16:00 p.m., where the maximum value, 82%, was seen in the morning then falls to 52% in the evening.

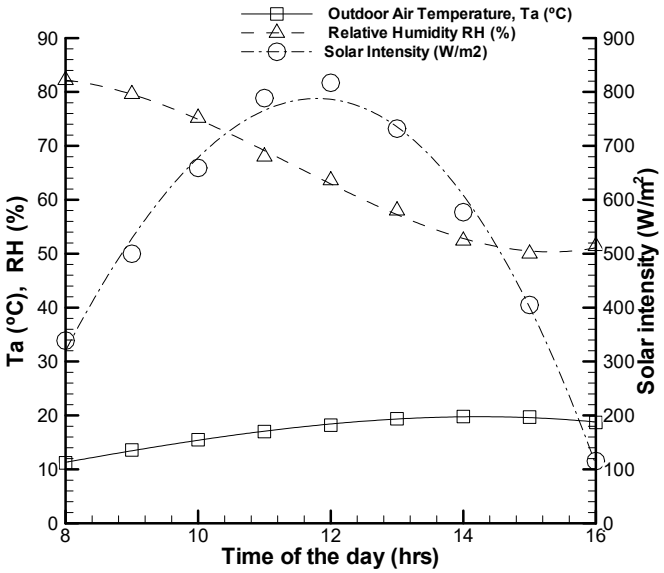

Figure 3. The average outdoor temperatures were associated with solar intensity and humidity ratio.

4.2. Inlet Temperature, Bed Temperature and Outlet Temperature

Figure 4 illustrates the ambient temperature (T_a), inlet temperature (T_i), bed temperature (T_b) and outlet temperature (T_o), with the time of the day from morning 08:00 to evening 16:00, for five different air flow rate from 0.003 kg/s to 0.018 kg/s. Temperature curves (T_a), (T_i), (T_b) and (T_o) had a similar manner with the solar intensity, increased to the maximum value at noon then decreased at the end of the day. The inlet air temperature (T_i) was higher than the ambient temperature (T_a). The ambient temperature was measured at a shadow place nethermost the bed, while (T_i) measured at entrance of the bed. The outlet temperatures (T_o) were greater than bed temperatures (T_b), (bed temperature means the temperature of the passing air inside the bed at the middle), for all days of experiments. This behavior was due to the double-pass of unglazed collectors or the counter-flow, which means that the passing air was preheated in the upper channel before the air flow reversed direction to enter the lower channel. Furthermore, (T_b) and (T_o) increase as the air flow rate was decreased from 0.003 kg/s to 0.018 kg/s, mainly due to the increase in the time of the moving air through the collector (from inlet section to the end of the collector). In other words, the air was able to carry more heat from the perforated plate and the wire mesh. Table 2 present the average value of inlet temperature, bed temperature, outlet temperature, and solar intensity with different air flow rate.

Table 2. The average value of the solar intensity (I), ambient temperatures (T_a), bed temperatures (T_b) and outlet temperatures (T_o) with different air flow rate.

$\dot{m}$ kg/s	I avr. W/m²	$T_{a\ avr.}$ °C	$T_{b\ avr.}$ °C	$T_{o\ avr.}$ °C	$\Delta T_{avr.}$ °C
0.003	661.0	17.7	49.4	56.3	38.6
0.005	627.6	17.8	47.7	54.4	36.5
0.013	510.9	14.5	46.0	51.1	33.2
0.016	426.1	17.2	35.6	40.5	26.0
0.018	598.8	17.8	33.5	37.5	20.3

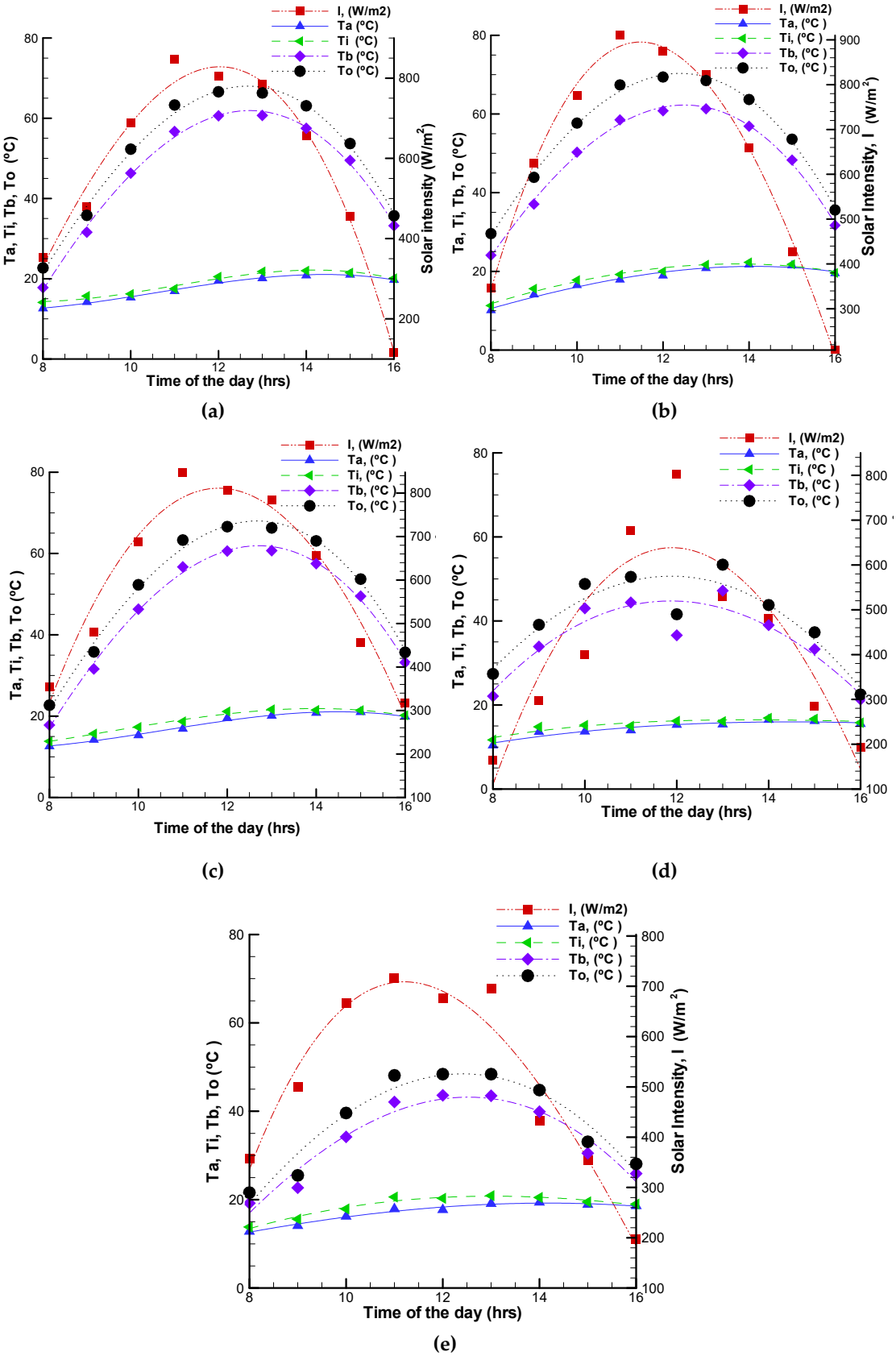

Figure 4. Inlet temperature, bed temperature, outlet temperature and solar intensity for: (**a**) Day 1: m = 0.003 kg/s; (**b**) Day 2: m = 0.005 kg/s; (**c**) Day 3: m = 0.013 kg/s; (**d**) Day 4: m = 0.016 kg/s; (**e**) Day 5: m = 0.018 kg/s.

4.3. Temperature Differences between the Outlet and Inlet Temperatures ΔT

Figure 5 shows the temperature differences ($\Delta T = T_o - T_a$) with time, for different air flow rate (from 0.003 kg/s to 0.018 kg/s) increased from the morning at 08:00 to reach a maximum temperature at noon, then afternoon the (ΔT) slowly decreased to the end of the day at 16:00. The maximum temperature differences (ΔT) is obtained 52.5°C with a solar intensity of 925 W/m^2, at an air flow rate of 0.003 kg/s, where the (T_o) of the flowing air through the collector increased with decreasing airflow rate

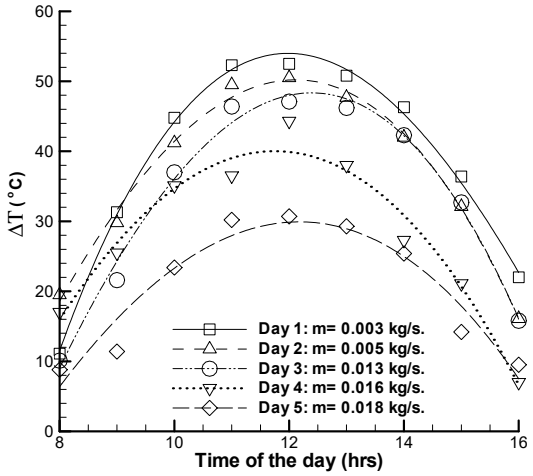

Figure 5. Temperature differences between the outlet and inlet temperature with the time of the day.

The results of temperature differences (as shown in Table 1) was compared with the previously unglazed transpired collectors published data, there was an enhancement in the heat transfer performance. The study of Kutscher [11] was obtained a maximum (ΔT) of 32 °C for at I = 700 W/m^2 for an air flow rate of 0.02 kg/s and perforated absorber area of 3 m × 3 m. The research [28], for numerical values, obtained, by neglecting the natural convection loss have obtained a maximum (ΔT) of 35 °C for at I = 800 W/m^2, air flow rate of 0.015 kg/s and perforated absorber area of 2 m × 3 m. Rad and Ameri [29] obtained the highest (ΔT) of 15 °C with a bed area of 2.79 m × 1.5 m at an air flow rate of 0.02 kg/s and I = 800 W/m^2. Theoretical and experimental investigated [30], for unglazed perforated solar air collector, which is coupled to a capillary heating system, the (ΔT) of 14.7 °C for ambient temperature (T_a) of 10 °C at $\dot{m}$ = 0.005 kg/s, and bed area of 1.2 m × 2.2 m.

4.4. Thermal Efficiency (η)

From Equation (4), if the efficiency is plotted against the temperature parameter $(T_i - T_a)/I$, a straight line was made where the slope is indicative of (U_L), and the y-intercept is indicative of ($\tau\alpha$). In fact, (U_L) is not a constant, but a function of the ambient temperature and the outlet temperature of the collector. Figure 6 presents the instantaneous thermal efficiency (η_i) of the collector versus $(T_i - T_a)/I$, for air flow rate of 0.018 kg/s. The maximum efficiency gained 86%, for air flow rate 0.018 kg/m^2 (Day 5), with the negative linear fit behavior slope B = −1.1782 and a correlation coefficient R^2 = 0.5566. The temperature parameter $(T_i - T_a)/I$ is increased as the thermal efficiency decreased, increasing of $(T_i - T_a)/I$ caused an increase in the heat loss from the upper cover to the surrounding, thus, thermal efficiency is reduced. There was a fluctuation of thermal efficiency value during Day 4, due to the part cloudy day, that effect on the solar intensity and thermal efficiency of the collector. Thus, the slope of the curve Day 4 seems straight line or low slope (not like other days), the constant A and B, are higher than constant A and B for Days 1–3, and 5.

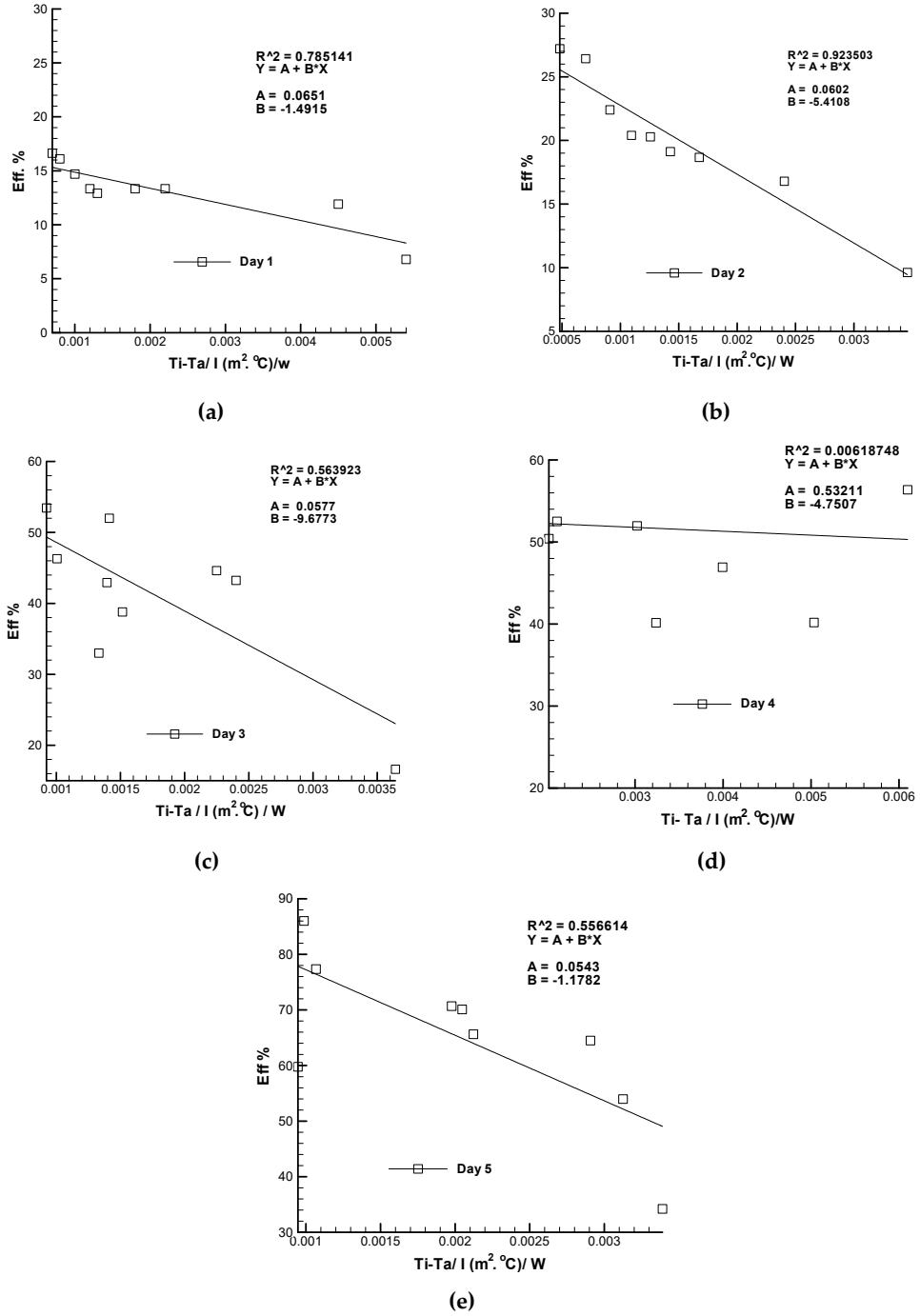

Figure 6. Instantaneous thermal efficiency (ηi) of the collector versus ($T_i - T_a$)/I, (**a**) air flow rate 0.003 kg/s; (**b**) air flow rate 0.005 kg/s; (**c**) air flow rate 0.013 kg/s; (**d**) air flow rate 0.016 Is; (**e**) air flow rate 0.018 kg/s.

The obtained empirical expression:

$$\eta_i = -1.4915\frac{(T_i - T_a)}{I} + 1.6361 \quad (5)$$

Replacing the slope by B and the origin by A, we obtain

$$\eta_i = -B.\frac{(T_i - T_a)}{I} + A \quad (6)$$

Adding Equations (6) and (3), we find the expression for (T_o) as a function of inlet air temperature (T_i) and the ambient temperature (T_a):

$$T_o = (1 - B\lambda)T_i + B\lambda T_a + AI\lambda \quad (7)$$

where the variable λ is defined as:

$$\lambda = \frac{A_c}{\nu A_e \rho C_p} = \frac{A_c}{\dot{m} C_p} \quad (8)$$

Replacing in Equation (7) the values of B, A and λ of our prototype, the model for the tested counter-flow, a double-pass solar collector is:

$T_o = 0.3443\ T_i + 0.6557\ T_a + 0.0651\ I$ (for Day 1 at m = 0.003 kg/s)

$T_o = -0.5392 T_i + 1.5932\ T_a + 0.0602\ I$ (for Day 2 at m = 0.005 kg/s)

$$T_o = -0.1414 T_i + 1.1414\ T_a + 0.0577\ I \text{ (for Day 3 at m = 0.013 kg/s)} \quad (9)$$

$T_o = 0.5477\ T_i + 0.4523\ T_a + 0.5321\ I$ (for Day 4 at m = 0.016 kg/s)

$T_o = 0.9954\ T_i + 0.0046\ T_a + 0.0541\ I$ (for Day 5 at m = 0.018 kg/s)

If the ambient temperature was the same inlet temperature ($T_a = T_i$), then Equation (9) given as:

$T_o = T_a + 0.0651\ I$ (for Day 1 at m = 0.003 kg/s)

$T_o = T_a + 0.0602\ I$ (for Day 2 at m = 0.005 kg/s)

$$T_o = T_a + 0.0577\ I \text{ (for Day 3 at m = 0.013 kg/s)} \quad (10)$$

$T_o = T_a + 0.5321\ I$ (for Day 4 at m = 0.016 kg/s)

$T_o = T_a + 0.0541\ I$ (for Day 5 at m = 0.018 kg/s)

Figure 7 shows experimental outlet temperatures (T_o, Measured) and simulated temperatures (T_o, Simulated) versus hours of the day at different airflow rate, that given by Equation (10). Clear from Figure 7, there was a validation of the work conditions, for the double-pass, unglazed solar energy system. The different value between experimented and predicted data were between (0 to 5) °C, for all days of work. The experimental work and simulated work agreed. There was a mismatch between experimented and predicted curves, due to the outdoor work condition, that affected on the outlet temperature. They fluctuated for inlet temperature, solar intensity, wind speed and humidity are caused some unstable outlet temperature with time of the day.

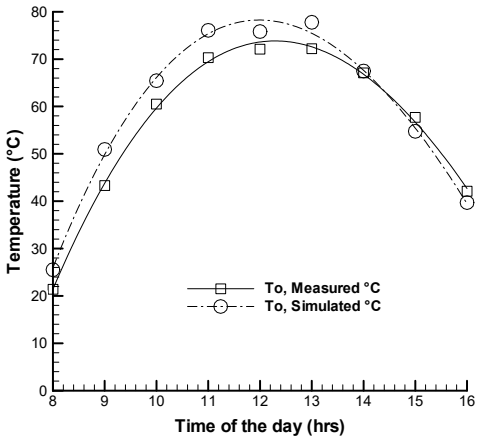

(a) Day 1: Airflow rate, 0.003 kg/s.

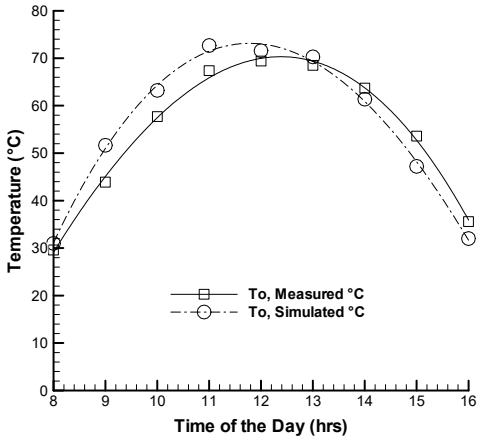

(b) Day 2: Airflow rate, 0.005 kg/s.

Figure 7. *Cont.*

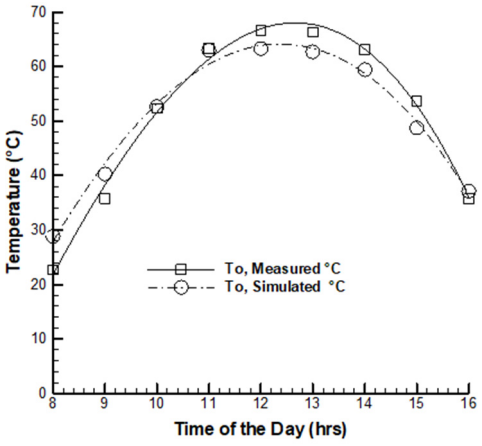

(c) Day 3: Airflow rate 0.013 kg/s.

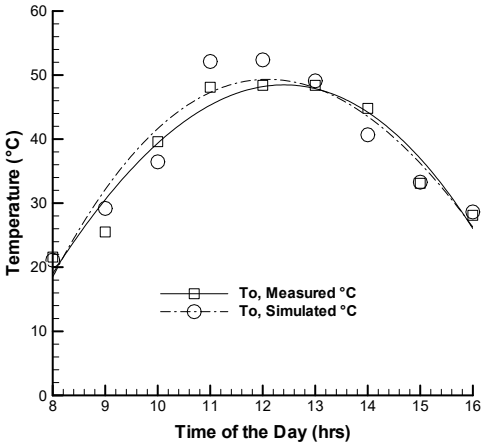

(d) Day 4: Airflow rate, 0.016 kg/s.

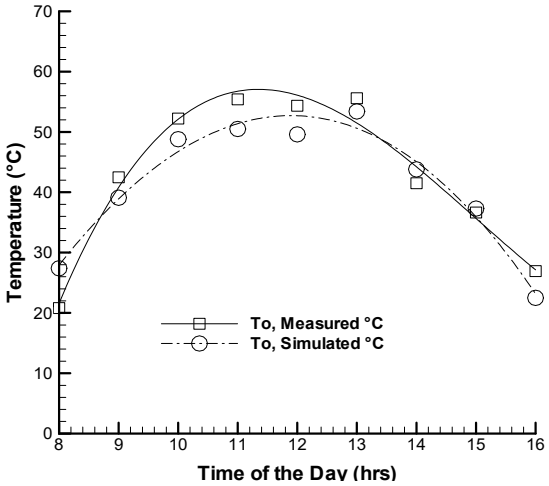

(e) Day 5: Airflow rate, 0.018 kg/s.

Figure 7. Experimented and predicted data of outlet air temperature for (**a**) Day 1; (**b**) Day 2; (**c**) Day 3; (**d**) Day 4 and (**e**) Day 5.

4.5. Effects of Airflow Rate

As estimated from Equation (3), the thermal efficiency of the collector can be improved by raising the air flow rate. The experimental results in Figure 8 show the thermal efficiencies for each day with different air flow rates raised from 0.003 kg/s to 0.018 kg/s. The weather condition of air inlet temperature (T_i) 21°C and the solar intensity 456 W/m^2. Evidently, there was a fluctuation of thermal efficiency value during Day 4, that was due to the partly cloudy, that effect on the solar intensity and efficiency for Day 4.

The high efficiency is caused by: First, the passing air through the upper channel is preheated the inlet air temperature before entering the bed. Second, the larger heat transferred between the passing air and absorber area (perforated plate and wire mesh layers). Third, the perforated plate acts as air jet impingement, the passing air through the hole enhancement the convective heat transfer.

The thermal efficiency in the present work was compared with the previously reported data. The proposed present new prototype of the unglazed solar collector showed significant improvement in the thermal efficiency, for air flow rate of 0.018 kg/s, as shown in Table 3.

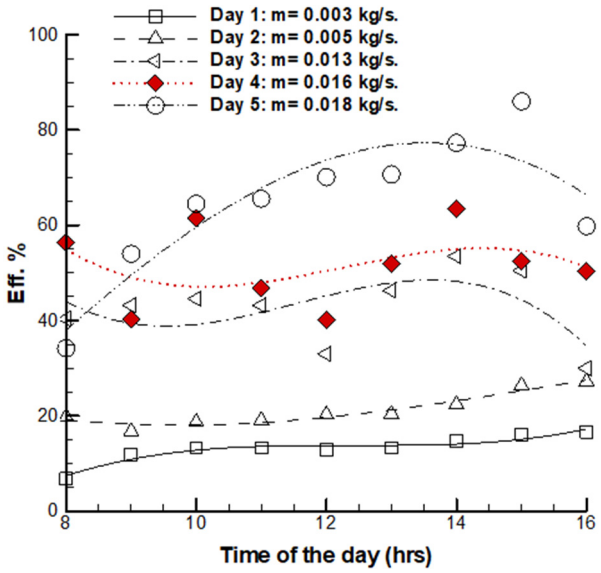

Figure 8. Variation of thermal efficiency at different air flow rates with the time of the day.

Table 3. Shows significant improvement in the thermal efficiency with for air flow rate (0.018 kg/s).

Researcher	Scheme	Type of Solar Collector (Description)	Area	Airflow Rate (kg/s)	η%
Kutscher et al. [10]	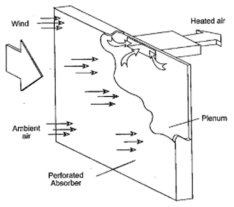	Perforated absorber plate and plenum between absorber plat and the south wall of the building.	9 m^2	0.018	76%
Mariana Gonzáleza et al. [16]	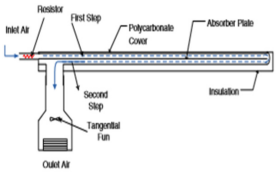	Unglazed solar collector Double flow collector, of Polycarbonate Cover and metal absorber.	2 m^2	0.02	45%
Gholampour [28]	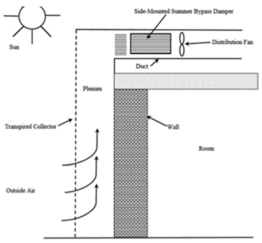	Perforated absorber plate and plenum between absorber plat and the south wall of the building.	6 m^2	0.018	75%
Present work	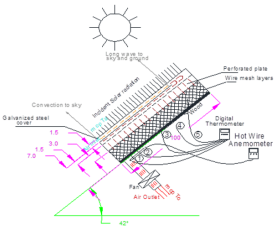	Unglazed solar collector, double-flow collector, with novelty of: (1) Two steel galvanized cover. (2) Perforated absorber plate. (3) Six wire mesh layers.	1.5 m^2	0.018	86%

As demonstrated in Figure 9, the efficiency increased continuously with the air flow rate, i.e., the heat transfer rate is directly proportional to the air flow rate. The increase in the air flow rate

increased the convection heat transfer coefficient, thus, enhancing the heat transfer from the collector to the working fluid. At the maximum air flow rate, 0.018 kg/s, the outlet temperature (T_o) was at the minimum value. By lowering the air flow rate the outlet temperature (T_o) increased, due to the increase in the time of moving air, the air took more time to move from the inlet section to the end of the collector. Thus, the air carried more heat from the perforated plate and the wire mesh layers. Therefore, the application of the solar energy system in cold weathers should be at a low air flow rate to satisfy the thermal comfort of the buildings. At the minimum air flow rate, 0.003 kg/s, the maximum average temperature difference ($\Delta T_{ave.}$), 38.6 °C, was achieved with average inlet temperature ($T_{a\ ave.}$) of 17.7 °C and average solar intensity ($I_{ave.}$) of 661 W/m^2 (Day 1 of the work).

$\dot{m}$ (kg/s)	T_a avr. (°C)	I avr. (W/m^2)	Eff. ave. %	ΔT ave. (°C)
0.003	17.7	661.0	13.2	38.6
0.005	17.8	627.6	21.2	36.5
0.013	17.8	598.8	42.7	33.2
0.016	17.5	510.9	51.5	26.0
0.018	14.2	426.1	64.7	20.3

(a)

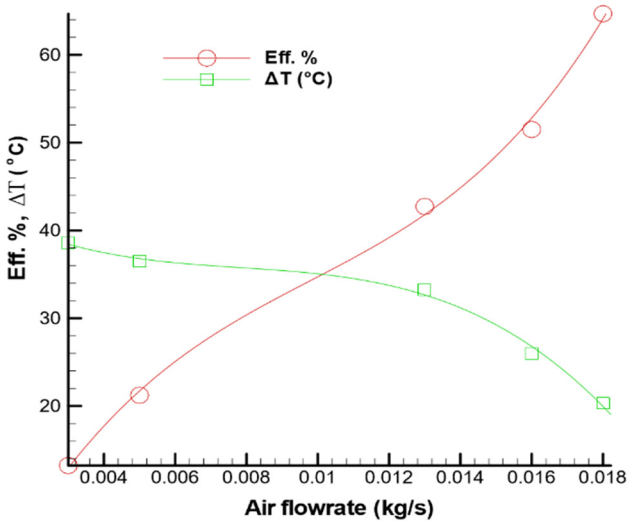

(b)

Figure 9. (**a**) Table of the average solar intensity and inlet air temperature, thermal efficiencies and temperature differences for five-day work; (**b**) variation of the average temperature differences and the average thermal efficiencies with the air flow rate for five-day work.

A solar energy system that is designed for high efficiency would have a high air flow rate and low outlet temperature. During low outside temperature (climate degree), the building manager would feel that the air is "cold" and think the collector is not working well. Thus, to ensure reaching the required level of heating, a conventional heater would need to be attached to the air flowing to the building. However, by setting the solar energy system for high-temperature, lower air flow rates should be used. This can satisfy the heating requirement of the building, but additional ventilation might be needed. An optimized level of air flow rate, that satisfies the requirements of the building for both heating and ventilation, should be the aim of the manager.

5. Conclusions

The experimental outdoor study of the outlet temperature and thermal efficiency of a double-pass unglazed solar air heater, with a perforated plate and wire mesh layers as an absorber plate, were complete. Afterwards, the prototype was designed and built in Baghdad, Iraq, to improve the conventional unglazed transpired collector for the new design of double plates cover of the unglazed solar energy system, during five cloudless winter days, with a maximum solar intensity on the collector cover plate of 925 W/m^2 and outdoor air temperatures ranging between 10–20 °C.

Ambient air temperatures were associated with humidity ratio and solar intensity—the ambient air temperature increased slightly from the morning, when the solar intensity increased. At the end of the day the solar intensity decreased to minimum value, while the ambient temperature at maximum value of (20 °C).

Temperature differences between the outlet and inlet temperatures with solar radiation curves increased when the air flow rate decreased. Outlet temperatures reached 72 °C at noon, with an average temperature rise of 52.5 °C, for an air flow rate of 0.003 kg/s.

Thermal efficiency was increased as the air flow rate increased from 0.003 to 0.018 kg/s. However, average daily efficiency of 64.7% was measured with an air flow rate of 0.018 kg/s.

Experimental results and the predictions of the theoretical model were complete, and agreed with the monitored data. The maximum different value between experimented and predicted data between 5 °C, for all days of work. For winter days, outlet temperature should be at least 45 °C, to ensure the thermal comfort of buildings in cold regions, so the optimal air flow rate used for this prototype research between 0.003 to 0.013 kg/s, providing an air outlet temperature of around 47–53°C.

A double-pass, counter-flow collector (to increase the air path, and therefore, gain more heat in addition to minimizing heat loss to the surroundings) was used to enhance the thermal performance. Non-uniform flow was obtained by passing air through wire mesh layers at the bottom part of the collector for increasing the absorbing heat. Suitable space heating and perfect preheating ventilation air required, if the ventilation air heated before entering the building.

Funding: This research received no external funding.

Conflicts of Interest: The authors declare no conflict of interest.

Nomenclature

A_c	absorbed area (m^2)
C_p	specific heat of air (kJ/kg K)
F_R	heat removal coefficient (-)
I	solar intensity (W/m^2)
k	air conductivity (W/m K)
$\dot{m}$	air flow rate (kg/s)
T_a	ambient temperature (°C)
T_b	air temperature inside collector (°C)
T_i	inlet air temperature (°C)
T_o	outlet air temperature (°C)
U_L	energy loss coefficient (kJ/m^2 K)
v	velocity (m/s)
η_i	instantaneous thermal efficiency (-)
η_{th}	thermal efficiency (-)
$\tau\alpha$	effective transmittance (-)
ρ	density (kg/m^3)

References

1. Kalogirou, S.A. Solar thermal collectors and applications. *Prog. Energy Combust. Sci.* **2004**, *30*, 231–295. [CrossRef]
2. Heiskanen, E.; Lovio, R.; Jalas, M. Path creation for sustainable consumption: Promoting alternative heating systems in Finland. *J. Clean. Prod.* **2011**, *19*, 1892–1900. [CrossRef]
3. Singh, S.; Dhiman, P. Using an analytical approach to investigate thermal performance of double-flow packed-bed solar air heaters with external recycle. *J. Energy Eng.* **2014**, *211*, 4001–4031. [CrossRef]
4. Naveed, A.T.; Kang, E.C.; Lee, E.J. Effect of unglazed transpired collector on the performance of a polycrystalline silicon photovoltaic module. *J. Sol. Energy Eng.* **2006**, *128*, 349–353. [CrossRef]
5. Vaziri, R.; Ilkan, M.; Egelioglu, F. Experimental performance of perforated glazed solar air heaters and unglazed transpired solar air heater. *Sol. Energy* **2015**, *119*, 251–260. [CrossRef]
6. Gao, L.X.; Bai, H.; Mao, S.F. Potential application of glazed transpired collectors to space heating in cold climates. *Energy Convers. Manag.* **2014**, *77*, 690–699. [CrossRef]
7. Zheng, W.; Li, B.; Zhang, H.; You, S.; Li, Y.; Ye, T. Thermal characteristics of a glazed transpired solar collector with perforating corrugated plate in cold regions. *Energy* **2016**, *109*, 781–790. [CrossRef]

8. Bhushan, B.; Singh, R. Thermal and thermohydraulic performance of roughened solar air heater having protruded absorber plate. *Sol. Energy* **2012**, *86*, 3388–3396. [CrossRef]
9. Kutscher, C.; Dymond, C. Development of a flow distribution and design model for transpired solar collectors. *Sol. Energy* **1997**, *60*, 291–300.
10. Kutscher, C.F.; Christensen, C.B.; Barker, G.M. Unglazed transpired solar collector: Heat loss theory. *Trans. ASME J. Sol. Energy Eng.* **1993**, *115*, 182–188. [CrossRef]
11. Kutscher, C.F. Heat exchange effectiveness and pressure drop for air flow through perforated plates with and without crosswind. *Trans. ASME J. Sol. Energy Eng.* **1994**, *116*, 391. [CrossRef]
12. Gunnewiek, L.H.; Brundrett, E.; Hollands, K.G.T. Flow distribution in unglazed transpired plate solar air heaters of large area. *Sol. Energy* **1996**, *58*, 221–237. [CrossRef]
13. Leon, M.; Kumar, S. Mathematical modeling and thermal performance analysis of unglazed transpired solar collectors. *Sol. Energy* **2007**, *81*, 62–75. [CrossRef]
14. Decker, G.W.E.; Hollands, K.G.T.; Brunger, A.P. Heat-exchange relations for unglazed transpired solar collectors with circular holes on a square or triangular pitch. *Sol. Energy* **2001**, *71*, 33–45. [CrossRef]
15. González, S.M.; Larsen, S.F.; Hernández, A.; Lesino, G. Thermal evaluation and modeling of a double-pass solar collector for air heating. *Energy Procedia* **2014**, *57*, 2275–2284. [CrossRef]
16. Adnane, L.; Noureddine, M.; Adel, B.; Kamel, A.; Abdelhafid, M. Performance investigation of single- and double-pass solar air heaters through the use of various fin geometries. *Int. J. Sustain. Energy* **2012**, *31*, 423–434.
17. El-Sebaii, A.A.; Abou-Enein, S.; Ramadan, M.R.I.; El-Bialy, E. Year-round performance of double pass solar air heater with a packed bed. *Conserv. Manag.* **2007**, *48*, 990–1003. [CrossRef]
18. Aldabbagh, L.B.Y.; Egelioglu, F.; Ilkan, M. Single and double-pass solar air heaters with wire mesh as packing bed. *Energy* **2010**, *9*, 3783–3787. [CrossRef]
19. Mahmood, A.J. Experimental Study of a solar air heater with a new arrangement of transverse longitudinal baffles. *ASME J. Sol. Energy Eng.* **2017**, *139*, 031004-1. [CrossRef]
20. Mahmood, A.J.; Aldabbagh, L.B.Y.; Egelioglu, F. Investigation of single and double pass solar air heater with transverse fins and a package wire mesh layer. *Energy Convers. Manag.* **2015**, *89*, 599–607. [CrossRef]
21. Sopian, K.; Supranto, W.R.; Daud, M.Y.; Othman, B.Y. Thermal performance of the double-pass solar collector with and without porous media. *Renew. Energy* **2013**, *18*, 557–564. [CrossRef]
22. Prashant, D.; Thakur, N.S.; Chauhan, S.R. Thermal and thermohydraulic performance of counter and parallel flow packed bed solar air heaters. *Renew. Energy* **2012**, *46*, 259–268.
23. Nowzari, R.; Aldabbagh, L.B.Y.; Egelioglu, F. Single and double pass solar air heaters with partially perforated cover and packed mesh. *Energy* **2014**, *73*, 694–702. [CrossRef]
24. Gawlik, K.; Christensen, C.; Kutscher, C. A numerical and experimental investigation of low-conductivity unglazed, transpired solar air heaters. *ASME J. Sol. Energy Eng.* **2005**, *127*, 153–155. [CrossRef]
25. Badache, M.; Rousse, D.R.; Hall, E.S.; Quesada, G. Experimental and numerical simulation of a two-dimensional unglazed transpired solar air collector. *Sol. Energy* **2013**, *93*, 209–219. [CrossRef]
26. Greig, D.; Siddiqui, K.; Karava, P. An experimental investigation of the flow structure over a corrugated waveform in a transpired air collector. *Int. J. Heat Fluid Flow* **2012**, *38*, 133–144. [CrossRef]
27. Wandong, Z.; Huan, Z.; Shijun, Y.; Yindan, F. Experimental investigation of the transpired solar air collectors and metal corrugated packing solar air collectors. *Energies* **2017**, *10*, 302. [CrossRef]
28. Gholampour, M.; Ameri, M. Design considerations of unglazed transpired collectors: Energetic and exergetic studies. *J. Sol. Energy Eng.* **2014**, *136*, 031004-1. [CrossRef]
29. Rad, H.M.; Ameri, M. Energy and exergy study of unglazed transpired collector- 2 stage. *Sol. Energy* **2016**, *132*, 570–586. [CrossRef]
30. Eryener, D.; Akhan, H. Theoretical and experimental investigation of perforated solar air collector coupled to a capillary radiant heating system. In Proceedings of the 9th International Conference on Heat Transfer Fluid Mechanics and Thermodynamics, Malta, 16–18 July 2012.